Earth and Planetary Science Letters 275 (2008) 32–42

Contents lists available at ScienceDirect

Earth and Planetary Science Letters

journal homepage: www.elsevier.com/locate/epsl

Constraints on lowermost mantle mineralogy and fabric beneath Siberia from seismic anisotropy

James Wookey *, J.-Michael Kendall

Department of Earth Sciences, University of Bristol, Wills Memorial Building, Queens Road, Bristol BS8 1RJ, UK

ARTICLE INFO

Article history:
Received 22 January 2008
Received in revised form 6 July 2008
Accepted 23 July 2008
Available online 21 September 2008

Editor: L. Stixrude

Keywords:
lowermost mantle
shear-wave splitting
post-perovskite

ABSTRACT

Seismic anisotropy is an important tool for studying the nature, origin and dynamics of the lowermost mantle (D''). Here we present analysis of the seismic anisotropy beneath Siberia from shear-wave splitting measured in ScS phases. Data come from two near-perpendicular raypaths (Hindu Kush to Northern Canada and the Kuril Arc to Germany; both at ~80° epicentral distance) with close ScS reflection points on the Core–Mantle boundary (CMB). We apply differential S–ScS splitting to minimise contamination from the source and receiver-side upper mantle. The two raypaths show different ScS splitting times and fast shear-wave orientations, incompatible with the VTI style of anisotropy inferred for much of the lowermost mantle. The availability of data at two azimuths give us an opportunity to better understand D'' anisotropy than in previous studies. For example, the results provide the first accurate measurement of the dip of the symmetry plane. Several mechanisms have been suggested to explain lowermost mantle anisotropy, including the lattice-preferred orientation of lower mantle minerals such as perovskite or post-perovskite, or the shape-preferred orientation of inclusions of melt. In order to infer the flow regime implied by these mechanisms we use elasticities from published deformation experiments to forward model shear-wave splitting. Tomography of the region suggests a north–south trend in the geodynamics, and a model incorporating post-perovskite with a [100](010) slip system or aligned melt inclusions are most naturally compatible with such a trend. This may suggest a connection with remnant slab material from past subduction in the north Pacific.

© 2008 Elsevier B.V. All rights reserved.

1. Introduction

The lowermost mantle (also known as D'') remains one of the most poorly understood parts of the deep Earth. It has been long recognised that this is an unusual region, with many anomalous seismic properties. This include upper and lower discontinuities which reflect both P- and S-waves (see Wysession et al., 1998 for review), regions of severely reduced velocities (Ultralow Velocity Zones – ULVZs – see Garnero et al., 1998 for review), scatterers (Thomas et al., 1999; Hedlin and Shearer, 2000; Braña and Helffrich, 2004) and evidence of chemical heterogeneity (Masters et al., 2000; Trampert et al., 2004).

The lowermost mantle also shows significant seismic anisotropy (the variation of seismic wavespeed with direction), with a magnitude only exceeded by that observed for the uppermost mantle. Seismic anisotropy is an indication of long range order in the deep Earth, and its measurement can provide both mineralogical and dynamical constraints. The most unambiguous evidence of anisotropy in body waves comes from the observation of shear-wave splitting. This phenomenon occurs when a shear-wave propagating through the Earth encounters an anisotropic medium. The shear-wave is split into two – orthogonally polarised – components whose orientations are defined by the symmetry of the medium. As they propagate they separate in time, and this time difference and the orientation of the two shear waves persist outside the anisotropic medium and can be measured at the surface. Shear-wave splitting in SKS phases, for example, is routinely used to study anisotropy in the uppermost mantle (see, e.g., Montagner, 1998; Savage, 1999; Kendall, 2000 for reviews).

Shear-wave splitting has also been extensively studied in body-wave phases which transit the lowermost mantle (for reviews see Lay et al., 1998; Kendall and Silver, 1998; Moore et al., 2004; Wookey and Kendall, 2007). The information we can obtain from such studies, however, is limited by the symmetry of anisotropy that can be resolved. The most commonly used procedure is to measure the travel-time difference between the radial and transverse components of phases such as S, ScS and Sdiff. This requires the assumption of vertically transverse isotropy (VTI, also called radial or polar anisotropy; see, e.g., Thomsen, 1986). This has proved useful for long-wavelength dynamical inferences (Panning and Romanowicz, 2004) but does not provide enough information to distinguish between mechanisms of anisotropy for the lowermost mantle. More recent studies have allowed for a more general symmetry of anisotropy: tilted transverse isotropy (TTI) (Garnero et al., 2004; Maupin et al., 2005; Wookey et al., 2005a; Rokosky et al., 2006; Thomas et al., 2007). This has allowed better resolution of more

* Corresponding author.
E-mail address: j.wookey@bristol.ac.uk (J. Wookey).

0012-821X/$ – see front matter © 2008 Elsevier B.V. All rights reserved.
doi:10.1016/j.epsl.2008.07.049

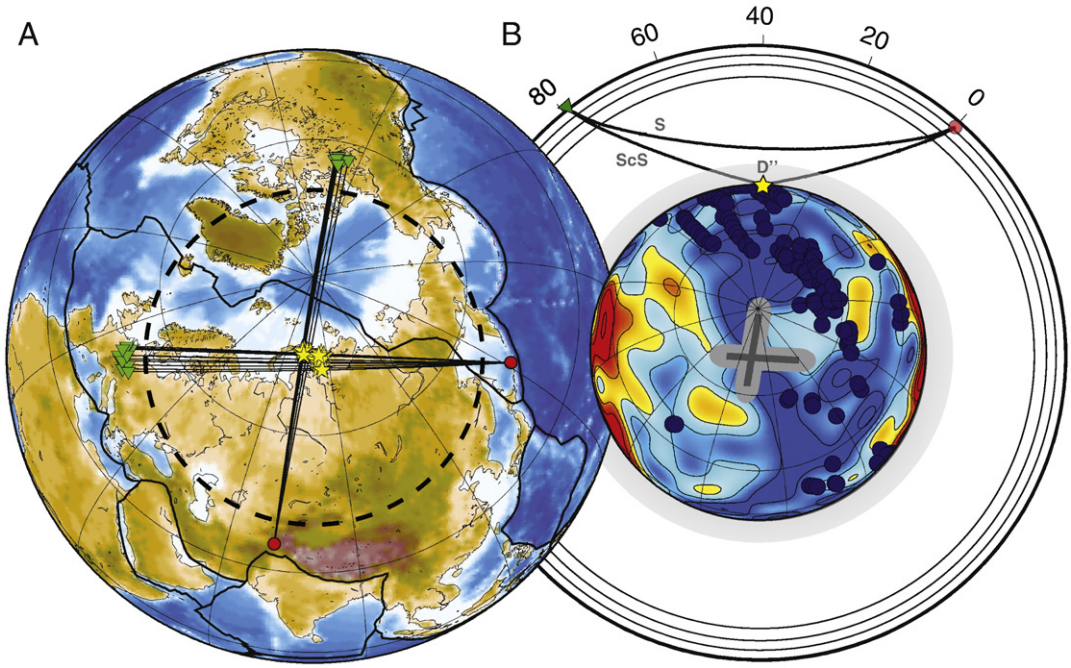

Fig. 1. Raypaths and bounce points for data used in the study. Panel A shows the great-circle paths for the phases studied, from Hindu Kush and Kuril Arc events (circles) to POLARIS and GRSN stations (triangles). Stars mark the reflection point of ScS: for both paths these are very close. Panel B shows the variation of shear-wave speed at the CMB from (Masters et al., 2000) (blue colours are faster than average) and the predicted location of paleosubducted slab material from (Lithgow-Bertelloni and Richards, 1998) (blue circles). The grey region shows the approximate Fresnel zone of the ScS phases in the lowermost mantle. Also shown are the S and ScS raypaths; S turns above D'' while ScS samples it.

localised dynamical features, but is still non-unique with regard to the mechanism causing the anisotropy.

Several explanations for D'' anisotropy have been suggested. Firstly, the anisotropy could be due to the lattice-preferred orientation (LPO) of $MgSiO_3$ in perovskite (e.g., Kendall and Silver, 1998; Stackhouse et al., 2005) or post-perovskite (Tsuchiya et al., 2004; Stackhouse et al., 2005) forms, or the alignment of MgO (Karato, 1998; Karki et al., 1999). $MgSiO_3$ is the most volumetrically important mineral in the lower mantle (e.g., ~80% in Pyrolite Ringwood, 1991).

Alternatively, the anisotropy could be explained by the shape-preferred orientation (SPO) of inclusions of subducted materials or melt (Kendall and Silver, 1996, 1998). These can display a strong anisotropic signature, even for very small volume fractions of included materials (Kendall and Silver, 1996; Moore et al., 2004). Candidate inclusion materials are molten remnant subducted basalts (Hirose et al., 1999) or iron from the core [e.g., (Wysession et al., 1998; Kanda and Stevenson, 2006)].

Obviously, the mechanisms outlined above provide a very wide spectrum of possible models of D'' anisotropy, and not knowing which is dominant makes robust dynamical inferences difficult. Apart from the need for more studies of the mineralogy and rheology of D'' minerals, progress will be made from seismic observations, particularly if we can design methods which allow us to resolve more complex symmetries of anisotropy. This is possible with improved azimuthal coverage of the lowermost mantle.

2. Dataset

In most regions of the lowermost mantle we are limited to one azimuth of observation, which places strong constraints on the complexity of anisotropy we can resolve. D'' beneath Siberia, however, offers the rare opportunity to image the anisotropy from two, nearly orthogonal directions; see Fig. 1 and (Thomas et al., 2002). Core reflected body-wave phases (e.g., PcP and ScS) from events beneath the Hindu Kush recorded at Canadian seismic stations have reflection points at the core–mantle boundary (CMB) very close to those for Kuril Arc events recorded in Northern Europe. Furthermore, the availability of array data from the POLARIS deployment in the Northwest Territories of Canada, and from the German Regional Seismic Network (GRSN) also gives the opportunity to develop new methodologies for resolving lowermost mantle anisotropy. From around 30 candidate events (predominantly on the Kurils–GRSN path) we have selected one from each direction with the clearest S, SKS and ScS arrivals (see Table 1). The availability of high quality data is somewhat limited by the short period of operation of the POLARIS array (from 2004 only), the relative infrequency of deep Hindu Kush earthquakes and a paucity of events showing clear S-waves from the Kuril Arc. Although further results might have been usable, their robustness was suspect, so we choose in this study to focus on our best data. Our stations are in a Δ=78–81° epicentral distance range in both directions (see Fig. 1 and Fig. 2).

3. Methodology

One of the major challenges in studying D'' anisotropy is correcting for the effect of the upper mantle, both beneath the station and in the region of the source. Recently, Wookey et al. (2005a) have introduced a technique which incorporates these corrections: S–ScS differential shear-wave splitting analysis.

This technique addresses the problem of interference from anisotropy in the vicinity of the source and the receiver by applying a 3-layer splitting approach. It is applicable to source–receiver pairs between Δ=60–85° epicentral distance. Example S and ScS raypaths

Table 1
Summary of ScS shear-wave splitting results

Path	Event date/time	Δ (°)	Baz. (°)	ϕ (°)	ϕ^* (°)	δt (s)	D'' ani. (%)
Hindu Kush–POLARIS	2004/04/05 21:24	79.2	358.4	−89±4	87	2.7±0.18	1.38±0.16
Kuril–GRSN	1996/02/22 14:59	79.2	27.7	−7±11	35	1.45±0.15	0.74±0.16

These show details of the two paths used, fast direction in a geographical (ϕ) and ray-oriented (ϕ^*) reference frames, splitting time (δt) and inferred anisotropy in the lowermost mantle (averaged over ScS path).

for an event at 79° calculated (Crotwell et al., 1999) for the reference model *ak135* (Kennett et al., 1995) are shown in Fig. 1. The S-phase turns above D'' while the ScS wave samples it; both have similar paths in the upper mantle and transition zone. The lower mantle region above D'' is generally considered to be isotropic (see, for example, Montagner, 1998; Kendall, 2000 for reviews). With distances >85° the S-phase begins to intersect the D'' discontinuity, and at distances <60° the raypaths become too separated in the upper mantle. It is also worth noting that in places where D'' is thinned (<~100 km), a strong SdS reflection this could potentially interfere with the ScS phase. Applying the array based technique outlined here can reduce this effect (by separating the phases in slowness), but caution is still merited. For the thickness of D'' beneath Siberia (200–300 km Thomas et al., 2002), ScS and SdS are separated by at least 10 s (in *ak135*).

Shear-wave splitting in the data is measured using the semi-automated method of Teanby et al. (2004) (an extension of the method of Silver and Chan, 1991). This method attempts to minimise the effect of anisotropy on a pair of horizontal seismograms by correcting for a range of possible lag-times (δt) and fast directions (ϕ), implemented as a grid search. For each pair of values (each node on the grid) the eigenvalues of the covariance matrix of the two horizontal components are calculated. The best-fitting δt and ϕ correspond to the node with the smallest λ_2 (the smallest eigenvalue). These parameters best linearise the ellipticity of the particle motion. The error in the results is estimated by applying a statistical F-test, and using the extent of the 95% confidence interval. The method incorporates analysis window optimisation based on cluster analysis (Teanby et al., 2004). We can also incorporate a source-side (Γ_S) and receiver-side (Γ_R) correction: Γ_R is applied before the analysis; Γ_S is applied during the analysis to every node in the grid search to preserve the commutation of the splitting operators (Wolfe and Silver, 1998).

To determine receiver (Γ_R) and source (Γ_S) terms we use stations with well-established SKS measurements. For the Kurils–Germany raypath we use BFO, GRFO and BRG. For these stations the splitting measured in the direct S-phase is very similar to published SKS results (Brechner et al., 1998; Thomas and Kendall, 2002; Evans et al., 2006) at similar polarisations, implying a negligible contribution from source-side anisotropy. This need not necessarily mean that no anisotropy is present in the Kurils Arc subduction zone near the source: it may be that the source polarisation is such that no splitting results (i.e., if the polarisation is near-parallel or perpendicular to the fast direction). In either case there is no requirement for a source-side correction of ScS. The source polarisation (~322° in the source reference frame) is similar to the trench perpendicular direction. Thus trench parallel anisotropy will cause no splitting: a reasonable possibility which is compatible with observations at (relatively) nearby stations (Fouch and Fischer, 1996; Long and van der Hilst, 2005). However, the S-phase used also rapidly exits the subducting slab at the back-azimuth of our stations, and so it is also possible that almost no anisotropy affects the phase. We cannot distinguish these two scenarios, but neither affect how we need to treat the data. The next step is to determine a

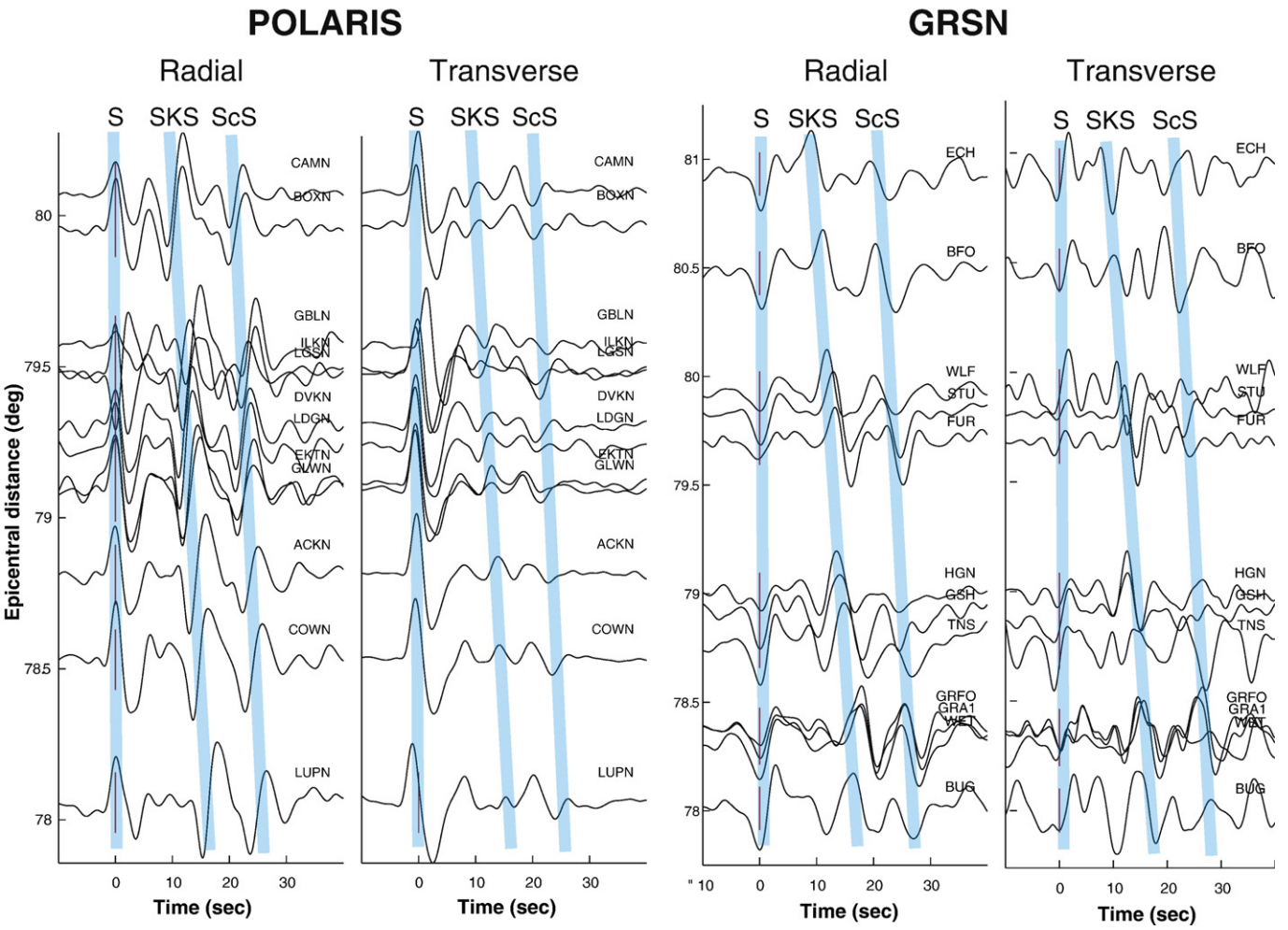

Fig. 2. Record sections of data used. Radial and transverse components of POLARIS (left panels) and GRSN (right panels), aligned on the peak of the S-wave arrival. The Canadian seismic records are in general less noisy, however the phases of interest are visible in the all data.

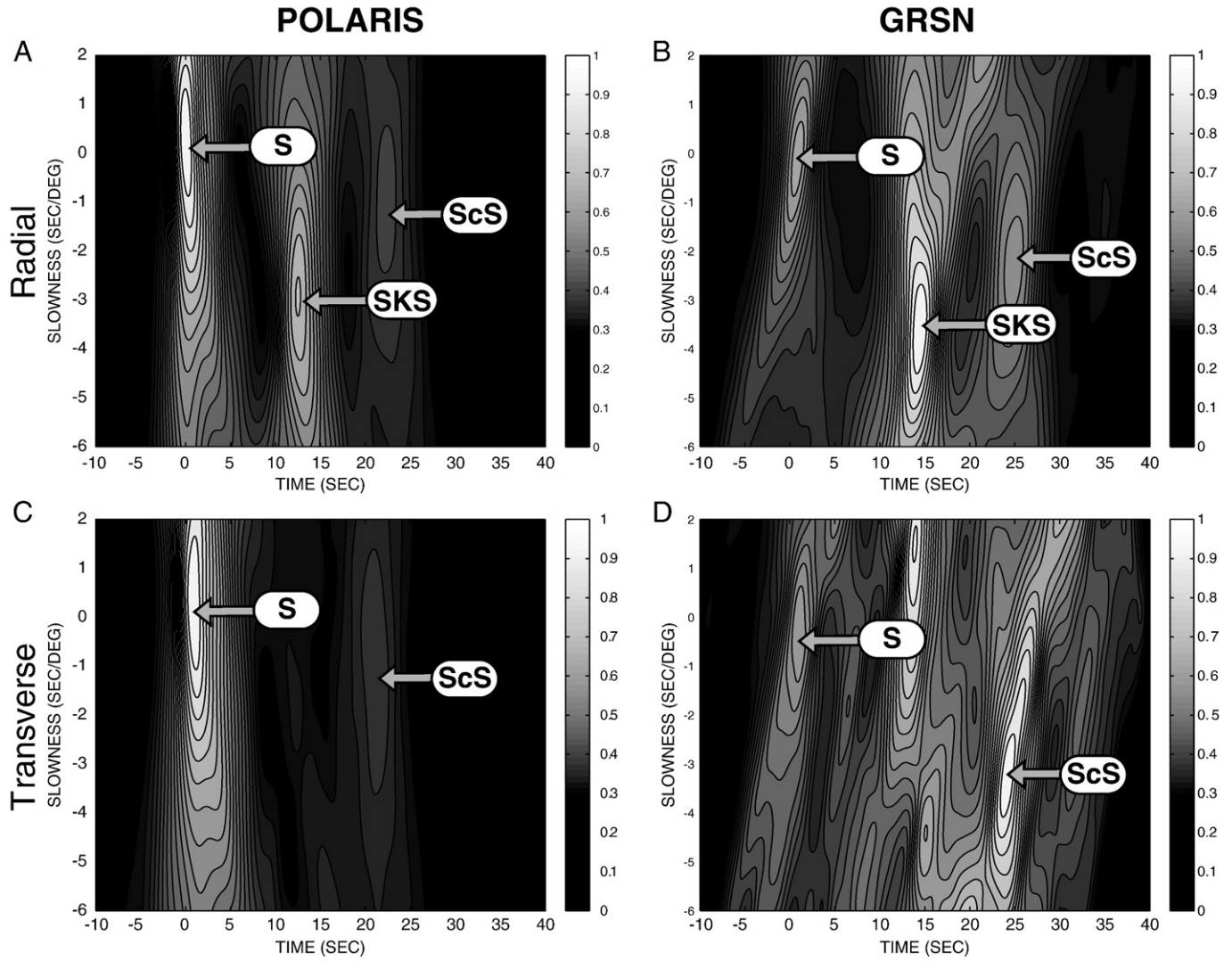

Fig. 3. Slant stacking POLARIS and GRSN array data. The left column shows the POLARIS results, and the right the GRSN. Panels A–D show the results of the slant stack, with an envelope function applied to make phase identification simpler. The S, ScS and SKS phases are clear on the radial components (panels A and B), while the SKS is absent from the transverse (panels C and D), removed by the correction for upper mantle anisotropy. Slant stacking allows us to improve signal to noise and separate the ScS phase from the other phases.

receiver-side correction for all the stations in the GRSN array. This is done by analysing splitting in the S-phase at all stations (since we have ruled out a source-side anisotropy contribution).

The POLARIS stations are somewhat more challenging. A recent SKS study (Snyder and Bruneton, 2007) of these stations strongly suggest two layers of anisotropy in the lithosphere. Initial measurements of the S-phase splitting suggested similar anisotropy to the upper layer in (Snyder and Bruneton, 2007); with a source polarisation similar to the fast direction of the lower layer. This explains why this did not affect the S-phases, however, the same could not necessarily be assumed for the ScS (as the splitting at the CMB may change the effective polarisation). Instead we use the parameters of the two layer model of (Snyder and Bruneton, 2007) to use as receiver-side correction for the POLARIS stations. These splitting operators were different enough from initial measurements of the direct S-phase to also suspect a non-negligible contribution from near-source anisotropy.

The dense spacing of the array stations means that the raypaths of the ScS phases in the lowermost mantle are close enough together that we may assume that they are sensitive to the same anisotropy and will have the same shear-wave splitting. This allows us to stack the data to improve signal to noise and to better separate the phases. This is done by means of a linear slant stack (Hake, 1998), see Fig. 3. We can then identify the peak slowness of S and ScS and form a single stacked trace for each component of each phase. We use a linear stack to avoid possible waveform contamination. We then analyse the splitting in these summed traces. Firstly, we measure the splitting in stacked S-phase for the Hindu Kush–Canada path. Since we have corrected for receiver-side splitting, any residual anisotropy may be reasonably attributed to splitting in the source region. In fact, we observe about 1 s of residual splitting in the stacked S-trace (see Fig. 4). The fast direction is roughly NE–SW (54±8°, projected onto the surface). This is very similar to the fast direction (60° measured for SKS at station KAAO (Kabul, Afghanistan; located approximately 200 km away from the event epicentre) (Vinnik et al., 1992), paralleling the main structural trend of the Hindu Kush mountain belt. The magnitude of splitting (~1 s) is almost half the SKS splitting observed at KAAO, implying consistent fabric deep into the upper mantle (the event depth is 180 km). We can use this source term to correct the ScS phase, providing two well-resolved measurements of lowermost mantle anisotropy at two nearly orthogonal azimuths.

4. Results

Fig. 5 shows the results of the ScS splitting in the two paths. The N–S (Hindu Kush–Canada) path shows a splitting time (δt) 2.7±0.18 s of

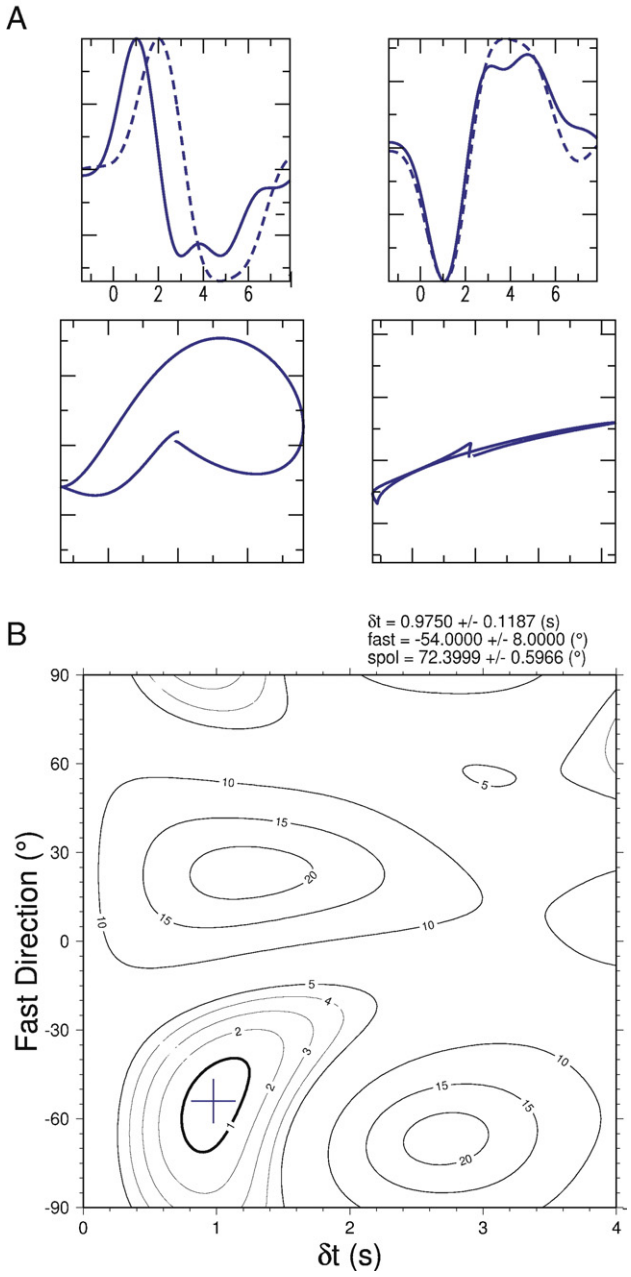

Fig. 4. Residual splitting in the (stacked) direct S-wave (Hindu Kush to Canada raypath) after correction for receiver-side anisotropy. Panel A shows the pre- (left) and post- (right) correction waveform (top) and particle motion. Panel B shows the associated error surface: the best-fitting splitting operator is ϕ=−54±8°, δt=0.98±0.1 s. We attribute this to anisotropy in the source region.

splitting with a fast shear-wave polarisation (ϕ) of −89±4°; the (E–W) Kurils–Germany path δt=1.45±0.15 s and ϕ=−7±11°. Since the ScS phase is close to horizontal through the *D″* region at these distances (see Fig. 1), we interpret ϕ in terms of the orientation of the fast shear-wave in the plane defined by the vertical and transverse directions (i.e., back-azimuth minus ϕ, which we denote ϕ*; see Fig. 6. These are 89° and 35° for the two paths respectively. If we assume an average *D″* thickness in the region of 260 km (Thomas et al., 2002) we can estimate the degree of anisotropy from the splitting times. These are 1.38±0.16% for the N–S path and 0.74±0.16% for the E–W. These are summarised in Table 1. These are compatible with the results found by Thomas and Kendall (2002) at very similar bounce points, who measure around 1 s of splitting assuming a VTI symmetry, since the effect of dipping anisotropy is to reduce the magnitude inferred by such a method (Wookey and Kendall, 2007).

5. Interpretation

In order to attempt to constrain the cause of the measured shear-wave splitting it is desirable to test what symmetry of anisotropy can reproduce our results. It is clear from the non-horizontal fast direction measured for the Kurils–Germany path that the shear-wave splitting in the lowermost mantle cannot be attributed to a simple vertical transverse isotropy (VTI) style of anisotropy, as has often been assumed in previous studies (see, e.g., Wookey and Kendall, 2007). Therefore the simplest model which might be compatible with this is transverse isotropy with a tilted axis of symmetry. Furthermore, it could also be explained by anisotropy with a lower order of symmetry (orthorhombic, monoclinic, etc.). We seek therefore to test a range of plausible models for *D″* anisotropy against our results.

Potential anisotropy causing mechanisms in the lowermost mantle are shape-preferred orientation (SPO) and lattice-preferred orientation (LPO). SPO anisotropy involves the preferential alignment of sub-seismic wavelength inclusions of material with contrasting elastic properties to those of the host matrix. If these materials are fluid, such as basaltic melt (Hirose et al., 1999) or liquid iron (e.g., Kanda and Stevenson, 2006), large shear-wave anisotropies might be observed (Kendall and Silver, 1998). In general these are assumed to result in a VTI-style medium (i.e., no variation of apparent anisotropy with azimuth), but might impose an azimuthal anisotropy if oriented by an inclined deformation flow (i.e., resulting in a tilted-transversely isotropic medium; TTI). Some laboratory results (on upper mantle minerals) have even shown that dipping melt inclusions are even possible for simple horizontal flow (Holtzman et al., 2003).

LPO anisotropy involves the preferential alignment of crystals of lowermost mantle minerals. Most crystals in nature have a degree of anisotropy and those thought to be present in the lower mantle are no exception. The most volumetrically important mineral is thought to be $MgSiO_3$, either with a perovskite or post-perovskite structure. Ab initio studies of these minerals at near-CMB pressures and temperatures provide an estimate of the elasticity of these minerals (Stackhouse et al., 2005; Wookey et al., 2005b; Wentzcovitch et al., 2006) which shows that they are significantly anisotropic. However, for an anisotropic fabric to develop a favourable deformation mechanism is required (dislocation rather than diffusion creep), see e.g., Wenk et al. (2006). Recent experimental evidence has suggested that $MgSiO_3$ post-perovskite does deform by dislocation creep and form a significant LPO (Merkel et al., 2006; Yamazaki et al., 2006). There is however, contention about what slip system it deforms by. Based on high pressure, low temperature experiments with $MgGeO_3$ and $MgSiO_3$ Merkel et al. (2006, 2007) infer a slip system of $[\bar{1}10](110)$, consistent with that inferred by some theoretical methods (Oganov et al., 2005). However, ambient pressure, high temperature experiments with $CaIrO_3$ by Yamazaki et al. (2006) yield a slip system of [100](010) – more consistent with structural considerations (Iitaka et al., 2004) – and supported by some recent theoretical calculations (Carrez et al., 2007). LPO formation has also been observed in experimental studies of MgO (Yamazaki and Karato, 2002). We can use the elastic constants calculated by these studies to see whether such a model is compatible with the anisotropy we measure, and what geometry of deforming flow it would require.

We consider four sets of elastic constants (see Table 2). The first are those for a simple TI medium parameterised by *ak135* (Kennett et al., 1995) wavespeeds and Thomsen parameters ϵ=γ=δ=0.1 (Thomsen, 1986). These represent anisotropy due to SPO-type models such as layering, aligned fluid inclusions or the TI aggregate of lowermost mantle minerals (mechanisms which we cannot distinguish between). The remaining sets are based on ab initio calculated elastic constants for MgO (Karki et al., 1999), $MgSiO_3$ perovskite (Wookey et al., 2005b),

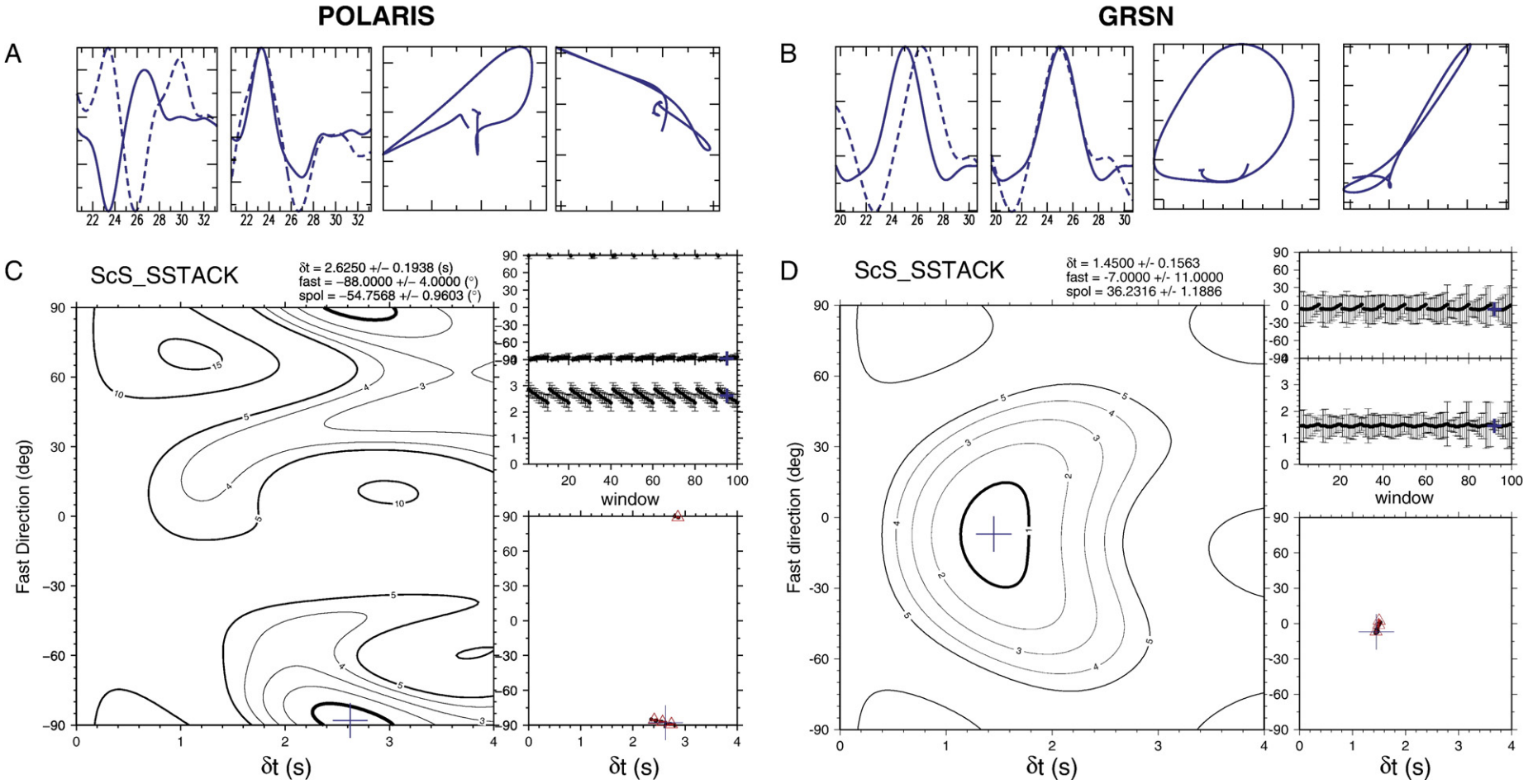

Fig. 5. Results of ScS shear-wave splitting analysis. Panels A–D show the results of the shear-wave splitting analysis on traces stacked at the peak slowness for ScS. Clear elliptical particle is shown to be corrected by the application of the best-fitting ϕ and δt (panels A+B). Panels C and D show the error surfaces and window analysis for the two shear-wave splitting results: $\phi = -89 \pm 4°$, $\delta t = 2.7 \pm 0.2$ s for POLARIS and $\phi = -7 \pm 11°$, $\delta t = 1.5 \pm 0.2$ s for GRSN. Both are well constrained by the 95% confidence interval (bold line).

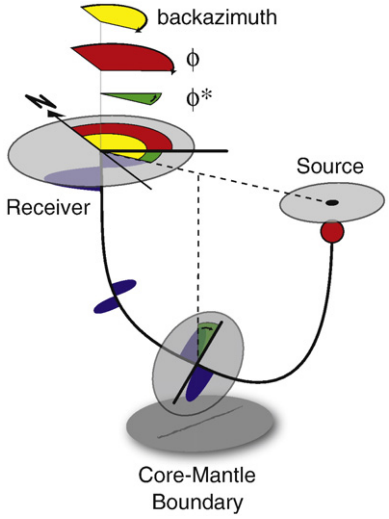

Fig. 6. Cartoon showing the relationship between recorded fast direction ϕ (in the geographical reference frame of the receiver) and ϕ^* (fast direction in a ray-based reference frame): ϕ^* is back-azimuth minus ϕ. The wavelet is the fast shear-wave; the slow wave is omitted for clarity. The bold vector is the projection of the fast S-wave onto the raypath normal plane. Since the ScS phase is near horizontal in the lowermost mantle, we interpret ϕ^*.

and $MgSiO_3$ post-perovskite (Stackhouse et al., 2005). In order to infer flow directions from these elastic constants we need estimates of the LPOs which develop under strain. The best source of these is from deformation experiments or calculations which determine orientations and perform averaging of the single crystal elastic constants to form an aggregate anisotropic fabric. These are available for MgO (Yamazaki and Karato, 2002), perovskite (Mainprice et al., 2008) and post-perovskite (Merkel et al., 2006; Yamazaki et al., 2006). We wish to test which, if any, orientation of these elastic constants are compatible with our results.

Arbitrary rotation of the elastic constants can be achieved by combinations of rotations about the three principal cartesian axes. We denote these angles α, β and γ for rotation about x, y and z respectively. We perform a grid search over these three angles, and for each node in the grid calculate the magnitude and orientation of shear-wave splitting using the Christoffel equation (see Wookey et al., 2005a) appendix for details). These are then compared with the anisotropy and polarisation measured in our data. Fig. 7 shows the orientations of these elastic constants which are compatible with our measured fast shear-wave polarisations: all models have some.

For the simple TI style anisotropy, only a single orientation fits. This is expected: with two polarisation vectors we define the symmetry plane. This model corresponds to a symmetry which dips 39.8±5° below horizontal at an azimuth of 178±8° (roughly south).

The high (cubic) symmetry of MgO means that a wide variation of orientations fit the measured polarisations. However, while our results are compatible with an LPO of MgO, the low volume fraction of this mineral mean that we do not favour it as an explanation: to achieve the anisotropy observed requires a high degree of alignment (and therefore strain). Both sets of perovskite elastic constants fit the data for a range of near-vertical shear planes. For post-perovskite with a [100](010) slip system (Yamazaki et al., 2006) both sets of results are similar, with southerly dipping shear and no constraint on direction. For a [$\bar{1}$10](110) (Merkel et al., 2006) slip system two orientations of dipping planes (both West–East and East–West) fit the measurements.

What is striking about these results is that none of the elastic constants are compatible on first sight with a horizontal shear plane, which one might expect for a simple, horizontal flow model for the lowermost mantle (assuming that shear planes align with the flow, not necessarily the case for complex poly-crystalline plasticity). It is, however, unsurprising that the lowermost mantle beneath Siberia might present a complex flow regime. Prolonged subduction in the northwest Pacific (>120 Myr) may imply the arrival of large amounts of slab material at the CMB in this region, associated with the Izanagi, Farralon, Kula and Pacific plates (Lithgow-Bertelloni and Richards, 1998; van der Voo et al., 1999). This is consistent with the increased

Table 2
Elastic constants tested

Model	MgO	MgO	VTI	Pv	Pv	PPv	PPv[a]	PPv[a]
	Low strain	High strain	–				Low strain	High strain
Ref.	Yamazaki and Karato (2002)	Yamazaki and Karato (2002)	–	Mainprice et al. (2008)	Mainprice et al. (2008)	Merkel et al. (2006)	Yamazaki et al. (2006)	Yamazaki et al. (2006)
P (GPa)	125	125	–	88	88	135	135	135
T (K)	0	0	–	1500	3500	4000	4000	4000
ρ (kg m^{-3})	5191	5191	5482	5031	4886	5262	5262	5262
C_{11} (GPa)	975	988	1226	955	827	972	1003	1005
C_{12}	456	426	534	394	368	420	413	418
C_{13}	422	440	541	387	359	411	418	417
C_{22}	980	1003	1226	920	808	985	994	993
C_{23}	417	425	541	367	345	412	416	421
C_{33}	1015	989	1021	898	798	1001	955	938
C_{44}	277	284	288	272	229	286	279	276
C_{55}	283	302	288	275	225	282	281	288
C_{66}	318	286	346	275	226	282	295	299
C_{14}	−6	−3	0	0	0	0	−1	−5
C_{15}	−19	−23	0	0	−1	16	0	1
C_{16}	0	−4	0	1	0	0	0	1
C_{24}	0	6	0	0	0	−1	2	3
C_{25}	−3	−1	0	−2	−2	−6	−2	−1
C_{26}	2	2	0	0	0	1	1	1
C_{34}	6	−1	0	0	0	1	4	3
C_{35}	24	25	0	−4	−1	14	−3	2
C_{36}	0	3	0	0	0	0	−1	0
C_{45}	0	3	0	0	0	0	0	0
C_{46}	−2	−1	0	0	0	7	−2	0
C_{56}	−6	−3	0	0	0	0	0	−4

Pressure and temperatures are those quoted for the single crystal elastic constants used to generate the aggregate tensor. Reference axes are: "1", shear-direction; "3", shear plane normal; and "2", perpendicular to "1" and "3".

[a] These elastic constants have been rotated to correct a deviation of the [100] from the slip plane of 30° and 15°, respectively; see (Yamazaki et al., 2006).

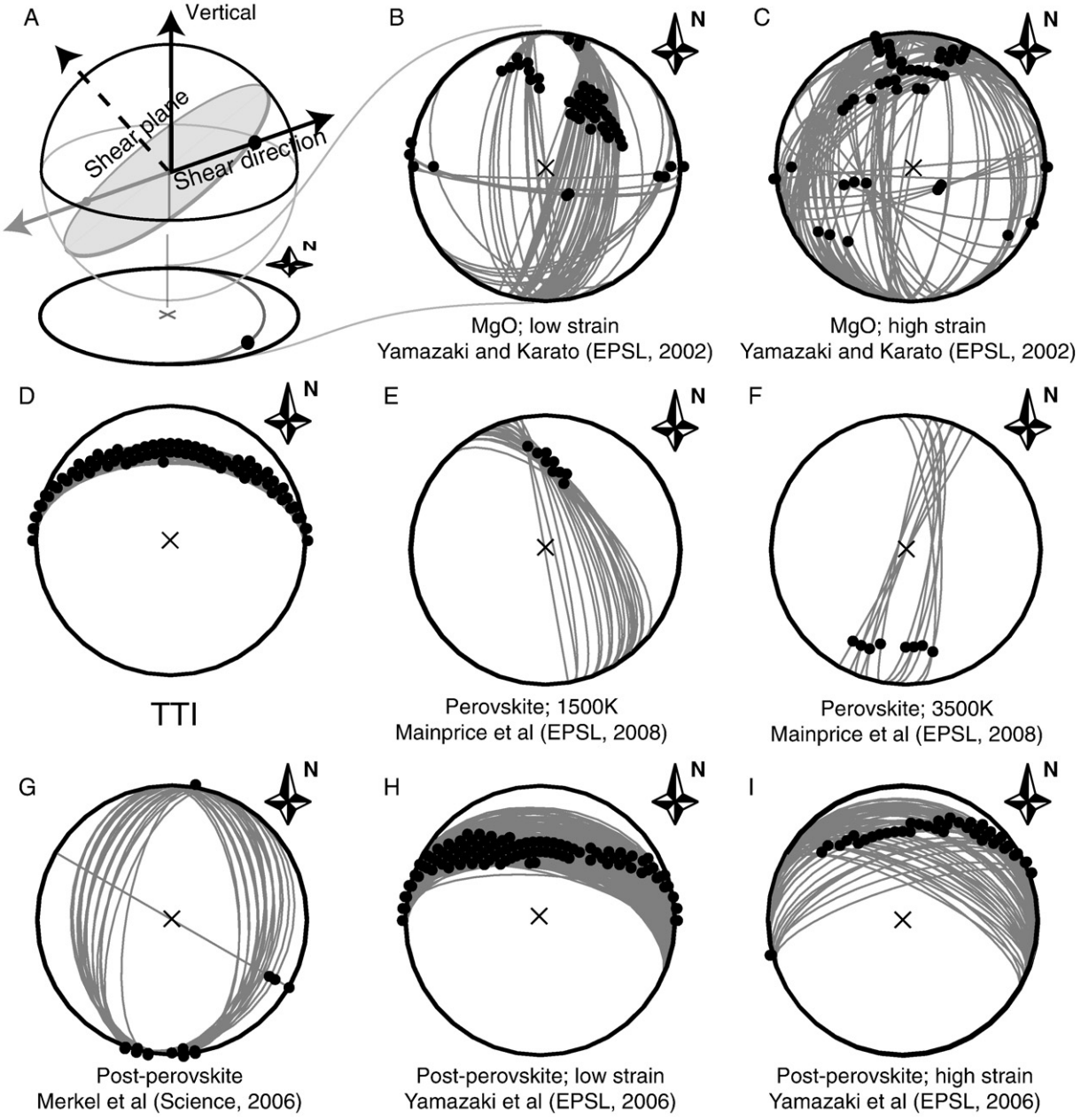

Fig. 7. Orientations of candidate elastic models which fit the shear-wave splitting observed beneath Siberia. Panel A is a cartoon showing how to interpret the other panels. Plots are upper hemispheric projections of the shear plane (grey arcs) and direction (black circles) predicted by matching orientations of different elastic tensors to the polarisations observed in the data. North is up the page, as indicated, and normal to the page is vertical (i.e., radially in the Earth). The elastic tensors tested are: B and C, an LPO of MgO from (Yamazaki and Karato, 2002); D, an ideal TTI medium (see text for details); E and F, $MgSiO_3$ perovskite from (Mainprice et al., 2008) at 1500 K and 3500 K; G, post-perovskite LPO using $MgGeO_3$ from (Merkel et al., 2006); H and I, post-perovskite LPO using $CaTiO_3$ from (Yamazaki et al., 2006).

seismic velocity in the region (see Fig. 1). Previous studies which have imaged the D'' discontinuity beneath Siberia have shown a highly contorted interface (Scherbaum et al., 1997; Thomas et al., 2002), with large lateral changes in inferred reflector depths. This has been interpreted as the effect of a 'pile-up' of remnant slab material. Seismic tomography in the region also shows a complicated picture. Fig. 8 shows shear-wave velocity variation in the locality of the ScS reflection point for three different tomographic models (Masters et al., 2000; Panning and Romanowicz, 2006; Montelli et al., 2006). Similarly to the discontinuity depth results this shows a complex picture with several apparent dipping structures in different orientations, with some differences between models. For example, only saw642an (Panning and Romanowicz, 2006) shows a distinct high velocity layer around D'' — interestingly this is the only model which incorporates anisotropy. All models, however, suggest a general transition from fast material south of the reflection point to slower, with less variation in the west–east transect. This suggests that the main geodynamic trend may also be north–south, though the precise geometry of any resulting flows is not constrained (previous studies have inferred buckling or reworking of subducted material (Scherbaum et al., 1997; Thomas et al., 2002). All of the models tested have valid north–south (or south–north) shear-directions; orientations of the shear planes most naturally compatible are TTI (and, hence, an SPO anisotropy with a dipping alignment) and post-perovskite with a [100](010) slip system (strike of the shear planes is perpendicular to N–S). Other models either have predominantly vertical shear planes (perovskite), or dip east–west (post-perovskite with a $[\bar{1}10](110)$ slip system). We cannot, given the complexity of the sub-Siberian

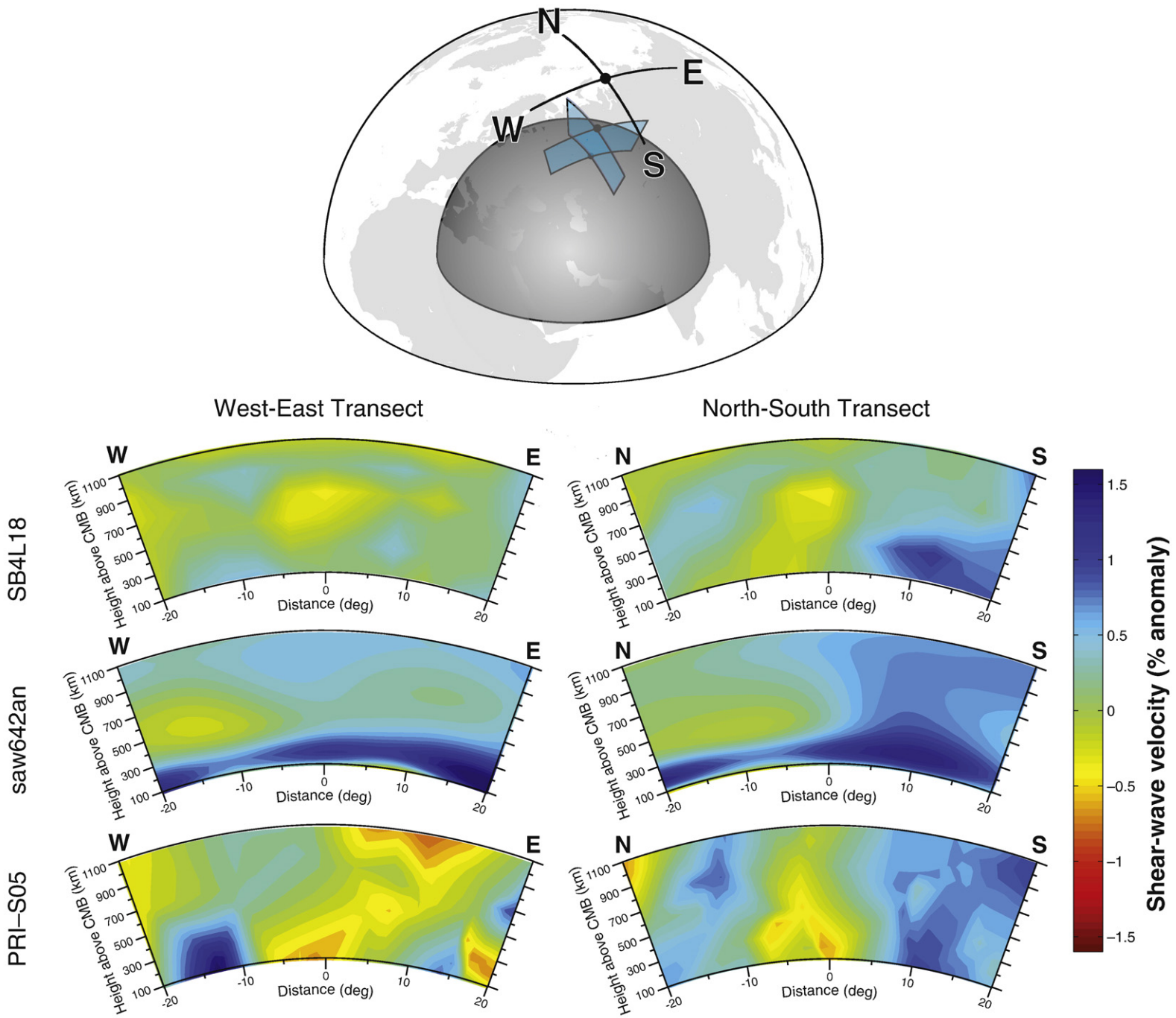

Fig. 8. Shear-wave tomography beneath Siberia. This shows velocities beneath Siberia from three tomography models: SB4L18 (Masters et al., 2000), saw642an (Panning and Romanowicz, 2006) and PRI-S05 (Montelli et al., 2006). Cross-sections along two transects are shown, cutting East–West and North–South through the average ScS reflection point for our events. Details differ between the models, but all models show complicated structure, with a general transition from south to north between fast and slow material.

lowermost mantle, definitely preclude these models but it seems reasonable to suggest that they are less likely explanations without additional constraints. Also, although it is a more minor component, MgO may still play a role. It might be possible to further refine these conclusions with more data, for example, extra azimuths to test; or using different phases such as Sdiff and SKS. The latter, however, would require more sophisticated forward modelling to be able to robustly compare.

6. Conclusions

We have presented the results of measuring D'' anisotropy beneath Siberia using differential S–ScS splitting. By using data from two different azimuths imaging the same region we are able — for the first time — to constrain both magnitude and dip of the anisotropy. A by-product of the process is an estimate of anisotropy in the Hindu Kush source region which agrees with nearby SKS results and the main structural trend of the mountain belt. In the lowermost mantle we show evidence of a dipping symmetry axis, a result which is incompatible with a simple VTI medium. Previous work measuring dipping anisotropy at a single azimuth (Garnero et al., 2004; Wookey et al., 2005a; Maupin et al., 2005; Rokosky et al., 2006; Thomas et al., 2007) must contend with a trade-off between dip extent and direction, preventing an accurate assessment of either and making comparisons with predictions from mineral physics difficult. With two azimuths we can make quantitative comparisons between our shear-wave splitting observations and those predicted by several plausible models of lowermost mantle anisotropy including the LPO of perovskite and post-perovskite. Even with measurements at two azimuths there is no single compatible mineralogy or orientation, however, all the models require a dipping shear plane. Tomography models in the region suggest an approximate north–south geodynamic trend, which is most naturally compatible with an SPO or post-perovskite explanation. However, reflector studies show that the sub-Siberian lowermost mantle is very complex, probably due to being the site of the arrival of subducted material for a prolonged period (>120 Myr). Extra azimuths, or different phases imaging the same region might help constrain the mineralogy further.

Acknowledgements

Data came from the CNSN and SZGRF data centres. The authors would like to thank Sebastién Merkel and David Mainprice for providing elastic constants from their papers; Mark Panning for the saw642an tomography model and Stephen Stackhouse, John Brodholt and David Price for helpful discussions. Two anonymous referees are thanked for thoughtful reviews, which have significantly contributed to the manuscript. JW was supported by a NERC fellowship grant.

References

Braña, L., Helffrich, G., 2004. A scattering region near the core–mantle boundary under the North Atlantic. Geophys. J. Int. 158, 625–636.
Brechner, S., Klinge, K., Kruger, F., Plenefisch, T., 1998. Backazimuthal variations of splitting parameters of teleseismic SKS phases observed at the broadband stations in Germany. Pure Appl. Geophys. 151 (2–4), 305–331.
Carrez, P., Ferré, D., Cordier, P., 2007. Implications for plastic flow in the deep mantle from modelling dislocations in $MgSiO_3$ minerals. Nature 446, 68–70.
Crotwell, H.P., Owens, T.J., Ritsema, J., 1999. The TauP toolkit; flexible seismic travel-time and ray-path utilities. Seismol. Res. Lett. 70 (2), 154–160.
Evans, M.S., Kendall, J.M., Willemann, R.J., 2006. Automated SKS splitting and upper-mantle anisotropy beneath Canadian seismic stations. Geophys. J. Int. 165 (3), 931–942.
Fouch, M.J., Fischer, K.M., 1996. Mantle anisotropy beneath northwest Pacific subduction zones. J. Geophys. Res. 101 (B7), 15,987–16,002.
Garnero, E.J., Revenaugh, J., Lay, T., Kellog, L.H., 1998. Ultralow velocity zone at the core–mantle boundary. In: Gurnis, M., Wysession, M.E., Knittle, E., Buffett, B.A. (Eds.), The Core–Mantle Boundary Region. Vol. 28 of Geodynamics, American Geophysical Union, pp. 319–334.
Garnero, E.J., Maupin, V., Lay, T., Fouch, M.J., 2004. Variable azimuthal anisotropy in Earth's lowermost mantle. Science 306, 259–261.
Hake, H., 1998. Slant stacking and its significance for anisotropy. Geophys. Prospect. 32, 828–850.
Hedlin, M., Shearer, P., 2000. An analysis of large-scale variations in small-scale mantle heterogeneity using global seismographic network recordings of precursors to PKP. J. Geophys. Res. 105, 13655–13673.
Hirose, K., Fei, Y., Ma, Y., Mao, H.K., 1999. The fate of subducted basaltic crust in the Earth's lower mantle. Nature 397, 53–56.
Holtzman, B.K., Kohlstedt, D.L., Zimmerman, M.E., Heidelbach, F., Hiraga, T., Hustoft, J., 2003. Melt segregation and strain partitioning: implications for seismic anisotropy and mantle flow. Science 301 (5637), 1227–1230.
Iitaka, T., Hirose, K., Kawamura, K., Murakami, M., 2004. The elasticity of the $MgSiO_3$ post-perovskite phase in the Earth's lowermost mantle. Nature 430 (6998), 442–445.
Kanda, R.V.S., Stevenson, D.J., 2006. Suction mechanism for iron entrainment into the lower mantle. Geophys. Res. Lett. 33 (3), L02310. doi:10.1029/2005GL025009.
Karato, S., 1998. Some remarks on the origin of seismic anisotropy in the D'' layer. Earth Planets Space 50 (11–12), 1019–1028.
Karki, B.B., Wentzcovitch, R.M., de Gironcoli, S., Baroni, S., 1999. First principles determination of elastic anisotropy and wave velocities of MgO at lower mantle conditions. Science 286, 1705–1707.
Kendall, J.M., 2000. Seismic anisotropy in the boundary layers of the mantle. In: Karato, S., Forte, A., Liebermann, R., Masters, G., Stixrude, L. (Eds.), Earth's Deep Interior: Mineral physics and Tomography From the Atomic to the Global Scale. Vol. 117 of Geophysical Monographs, American Geophysical Union, pp. 133–159.
Kendall, J.M., Silver, P.G., 1996. Constraints from seismic anisotropy on the nature of the lower mantle. Nature 381, 409–412.
Kendall, J.M., Silver, P.G., 1998. Investigating causes of D'' anisotropy. In: Gurnis, M., Wysession, M.E., Knittle, E., Buffett, B.A. (Eds.), The Core–Mantle Boundary Region. Vol. 28 of Geodynamics, American Geophysical Union, pp. 97–118.
Kennett, B.L.N., Engdahl, E.R., Buland, R., 1995. Constraints on seismic velocities in the Earth from traveltimes. Geophys. J. Int. 122 (1), 108–124.
Lay, T., Williams, Q., Garnero, E.J., Kellogg, L., Wysession, M.E., 1998. Seismic wave anisotropy in the D'' region and its implications. In: Gurnis, M., Wysession, M.E., Knittle, E., Buffett, B.A. (Eds.), The Core–Mantle Boundary Region. Vol. 28 of Geodynamics, American Geophysical Union, pp. 299–318.
Lithgow-Bertelloni, C., Richards, M.A., 1998. The dynamics of Cenozoic and Mesozoic plate motions. Rev. Geophys. 36 (1), 27–78.
Long, M.D., van der Hilst, R.D., 2005. Upper mantle anisotropy beneath Japan from shear wave splitting. Phys. Earth Planet. Inter. 151 (3–4), 206–222.
Mainprice, D., Tommasi, A., Ferre, D., Carrez, P., Cordier, P., 2008. Predicted glide systems and crystal preferred orientations of polycrystalline silicate Mg-Perovskite at high pressure: implications for the seismic anisotropy in the lower mantle. Earth Planet. Sci. Lett. 271 (1–4), 135–144.
Masters, G., Laske, G., Bolton, H., Dziewonski, A.M., 2000. The relative behaviour of shear velocity, bulk sound speed, and compressional velocity in the mantle: Implications for chemical and thermal structure. In: Karato, S., Forte, A., Liebermann, R., Masters, G., Stixrude, L. (Eds.), Earth's Deep Interior: Mineral physics and Tomography From the Atomic to the Global Scale. Vol. 117 of Geophysical Monographs, American Geophysical Union, pp. 201–213.
Maupin, V., Garnero, E.J., Lay, T., Fouch, M.J., 2005. Azimuthal anisotropy in the D'' layer beneath the caribbean, J. Geophys. Res. 110 (B8), B08301.
Merkel, S., Kubo, A., Miyagi, L., Speziale, S., Duffy, T.S., Mao, H., Wenk, H.R., 2006. Plastic deformation of $MgGeO_3$ post-perovskite at lower mantle pressures. Science 311 (5761), 644–646.
Merkel, S., McNamara, A.K., Kubo, A., Speziale, S., Miyagi, L., Meng, Y., Duffy, T.S., Wenk, H.R., 2007. Deformation of $(Mg,Fe)SiO_3$ post-perovskite and D'' anisotropy. Science 316 (5832), 1729–1732.
Montagner, J.P., 1998. Where can seismic anisotropy be detected in the Earth's mantle? In boundary layers. Pure Appl. Geophys. 151, 223–256.
Montelli, R., Nolet, G., Dahlen, F.A., Masters, T.G., 2006. A catalogue of deep mantle plumes: new results from finite-frequency tomography. Geochem. Geophys. Geosyst. 7 (11), 69.
Moore, M.M., Garnero, E.J., Lay, T., Williams, Q., 2004. Shear wave splitting and waveform complexity for lowermost mantle structures with low-velocity lamellae and transverse isotropy. J. Geophys. Res. 109, B02319.
Oganov, A., Martonak, R., Laio, A., Raiteri, P., Parrinello, M., 2005. Anisotropy of Earth's D'' layer and stacking faults in the $MgSiO_3$ post-perovskite phase. Nature 438 (7071), 1142–1144.
Panning, M., Romanowicz, B., 2004. Inferences on flow at the base of Earth's mantle based on seismic anisotropy. Science 303 (5656), 351–353.
Panning, M., Romanowicz, B., 2006. A three-dimensional radially anisotropic model of shear velocity in the whole mantle. Geophys. J. Int. 167 (1), 361–379.
Ringwood, A.E., 1991. Phase transformations and their bearing on the constitution and dynamics of the mantle. Geochim. Cosmochim. Acta 55, 2083–2110.
Rokosky, J., Lay, T., Garnero, E., 2006. Small-scale lateral variations in azimuthally anisotropic D'' structure beneath the Cocos Plate. Earth Planet. Sci. Lett. 248, 411–425.
Savage, M.K., 1999. Seismic anisotropy and mantle deformation: what have we learned from shear wave splitting? Rev. Geophys. 37, 65–106.
Scherbaum, F., Krüger, F., Weber, M., 1997. Double beam imaging: mapping lower mantle heterogeneities using combinations of source and receiver arrays. J. Geophys. Res. 102 (B1), 507–522.
Silver, P.G., Chan, W.W.J., 1991. Shear-wave splitting and subcontinental mantle deformation. J. Geophys. Res. 96, 16429–16454.
Snyder, D., Bruneton, M., 2007. Seismic anisotropy of the Slave craton, NW Canada, from joint interpretation of SKS and Rayleigh waves. Geophys. J. Int. 169 (1), 170–188.
Stackhouse, S., Brodholt, J.P., Price, G.D., Wookey, J., Kendall, J.M., 2005. The effect of temperature on the acoustic anisotropy of the perovskite and post-perovskite polymorphs of $MgSiO_3$. Earth Planet. Sci. Lett. 230 (1–2), 1–10.
Teanby, N.A., Kendall, J.M., Van der Baan, M., 2004. Automation of shear-wave splitting measurements using cluster analysis. Bull. Seismol. Soc. Am. 94 (2), 453–463.

Thomas, C., Kendall, J.M., 2002. The lowermost mantle beneath northern Asia — II. Evidence for lower-mantle anisotropy. Geophys. J. Int. 151 (1), 296–308.
Thomas, C., Weber, M., Wicks, C.W., Scherbaum, F., 1999. Small scatterers in the lower mantle observed at German broadband arrays. J. Geophys. Res. 104 (B7), 15,073–15,088.
Thomas, C., Kendall, J.M., Weber, M., 2002. The lowermost mantle beneath northern Asia; I, multi-azimuth studies of a *D″* heterogeneity. Geophys. J. Int. 151 (1), 279–295.
Thomas, C., Wookey, J., Simpson, M., 2007. *D″* anisotropy beneath Southeast Asia. Geophys. Res. Lett. 34 (4), L04301. doi:10.1029/2006GL028965.
Thomsen, L., 1986. Weak elastic anisotropy. Geophysics 51, 1954–1966.
Trampert, J., Deschamps, F., Resovsky, J., Yuen, D., 2004. Probabilistic tomography maps chemical heterogeneities throughout the lower mantle. Science 306 (5697), 853–856.
Tsuchiya, T., Tsuchiya, J., Umemoto, K., Wentzcovitch, R.M., 2004. Elasticity of post-perovskite $MgSiO_3$. Geophys. Res. Lett. 31 (14), L14603.
van der Voo, R., Spakman, W., Bijwaard, H., 1999. Mesozoic subducted slabs under Siberia. Nature 397 (6716), 246.
Vinnik, L., Makeyeva, L., Milev, A., Usenko, A., 1992. Global patterns of azimuthal anisotropy and deformations in the continental mantle. Geophys. J. Int. 111 (3), 433–447.
Wenk, H.R., Speziale, S., McNamara, A.K., Garnero, E.J., 2006. Modeling lower mantle anisotropy development in a subducting slab. Earth Planet. Sci. Lett. 245 (1–2), 302–314.
Wentzcovitch, R.M., Tsuchiya, T., Tsuchiya, J., 2006. $MgSiO_3$ postperovskite at *D″* conditions. Proc. Natl. Acad. Sci. 103 (3), 543–546.
Wolfe, C.J., Silver, P.G., 1998. Seismic anisotropy of oceanic upper mantle: shear wave splitting methodologies and observations. J. Geophys. Res. 103, 749–771.
Wookey, J., Kendall, J.M., 2007. Seismic anisotropy of post-perovskite and the lowermost mantle. In: Hirose, K., Brodholt, J., Lay, T., Yuen, D. (Eds.), Post-perovskite: The Last Mantle Phase Transition. Vol. 174 of Geophysical Monographs, American Geophysical Union, pp. 171–189.
Wookey, J., Kendall, J.M., Rümpker, G., 2005a. Lowermost mantle anisotropy beneath the north Pacific from differential S–ScS splitting. Geophys. J. Int. 161, 829–838.
Wookey, J., Stackhouse, S., Kendall, J.M., Brodholt, J., Price, G.D., 2005b. Efficacy of the post-perovskite phase as an explanation for lowermost-mantle seismic properties. Nature 438, 1004–1007.
Wysession, M.E., Lay, T., Revenaugh, J., Williams, Q., Garnero, E.J., Jeanloz, R., Kellog, L.H., 1998. The *D″* discontinuity and its implications. In: Gurnis, M., Wysession, M.E., Knittle, E., Buffett, B.A. (Eds.), The Core–Mantle Boundary Region. Vol. 28 of Geodynamics, American Geophysical Union, pp. 273–297.
Yamazaki, D., Karato, S., 2002. Fabric development in (Mg,Fe)O during large strain, shear deformation; implications for seismic anisotropy in Earth's lower mantle. Phys. Earth Planet. Inter. 131, 251–267.
Yamazaki, D., Yoshino, T., Ohfuji, H., ichi Ando, J., Yoneda, A., 2006. Origin of seismic anisotropy in the *D″* layer inferred from shear deformation experiments on post-perovskite phase. Earth Planet. Sci. Lett. 252, 372–378.